

Characteristics of Unsteady Flows around a Circular Cylinder with Simultaneous Multipoint Measurements of Pressure

by

Naotaka WATANABE^{*1}, Tomohiro FURUTA^{*2} and Yoko TAKAKURA^{*3}

(Received on Mar. 31, 2014 and accepted on Jul. 10, 2014)

Abstract

This study aims to investigate the unsteady characteristics of flows close to the critical state around a circular cylinder experimentally by simultaneous multipoint pressure measurements. For the measurements of pressure distribution, 128 holes are made spirally around the cylinder and each hole is connected through a vinyl tube to a semiconductor pressure sensor. For the range of Reynolds number, 1.4×10^5 to 5.5×10^5 , the following quantities are computed and analysed: unsteady and time-averaged distributions of pressure coefficients, instantaneous and time-averaged drag and lift coefficients, perturbation of the lift coefficient, and Strouhal number, etc. As results, characteristics of the unsteady flows have been captured in subcritical, critical, and supercritical states. Above all, the characteristics in the critical range have been presented.

Keywords: Circular cylinder, Multipoint pressure measurements, Critical state

1. Introduction

The cylinder is used in various fields including the engineering field because it is a basic shape in all structural things, and also flows about the cylinder have been investigated from the view point of fluid mechanics¹⁻⁴), for example, on detailed flow structure with separation and consequent flow-induced vibration.

At the present day, owing to the progress of large-scale computers, by use of the CFD (Computational Fluid Dynamics)⁵⁻⁶) it became possible to capture the structure of three-dimensional unsteady flows in detail and also to apply the computational results to engineering designs, but the computational results depend on the accuracy of numerical methods, grid fineness, and boundary conditions, etc. Therefore for flows including severe conditions such as transition, turbulence, and separation, the validation study would still need the proper experimental data.

Regarding critical flows with the severe conditions about the simple shape of a circular cylinder, study by Roshko⁷) is classical and his experimental data for surface pressure distribution have been cited in many text books, but in mean

values. Unsteady property of the flows has not been made fully clear still now.

In the series of authors' researches^{8,9}), unsteady flows have been investigated in the vicinity of the critical state around a circular cylinder experimentally by use of simultaneous multipoint pressure measurements¹⁰). In these experiments, pressures at 128 holes are simultaneously measured, and the case with such multipoints is very rare. In the first trial⁸), reliability was maintained only for Reynolds number less than 5×10^5 because of ability limit of pressure sensors used. In the next step⁹), the range of Reynolds number was expanded up to 5.5×10^5 by raising the performance with new sensors. Thus unsteady flows have been analyzed to grasp the characteristics in subcritical, critical, and supercritical states.

In this paper, in addition to the previous results, enhanced data analysis such as FFT and perturbation is shown to present the characteristic behavior in the vicinity of the critical state more in detail by simultaneous multipoint pressure measurements.

2. Experimental Setup

2.1 Large-scale low-speed wind tunnel

In the experiments the large-scale low-speed wind tunnel of Tokai University has been used. The wind tunnel is

*1 Graduate Student, Course of Mechanical Engineering
*2 Undergraduate Student, Department of Prime Mover Engineering
*3 Professor, Department of Prime Mover Engineering

single-return closed-circuit type with the open jet test section (Fig.1), where the ground board is set up between the nozzle exit and the collector of the wind tunnel (Fig.2). The dimension of the test section is 1 m high, 1.5 m wide and 2 m long, and the wind speed range is 0 to about 40 m/s.

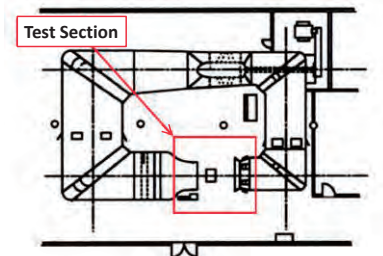


Fig.1 Wind tunnel of Tokai University



Fig.2 Ground board and test section

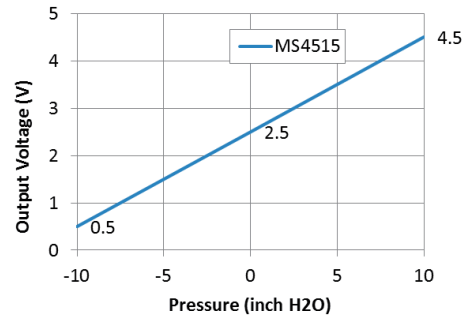
2.2 Device for simultaneous multipoint pressure measurements

Here the semiconductor pressure transducer, sensor MS4515 (Measurement Specialities Inc.), is adopted, and its output range in Voltage is shown in Fig.3. There are 2 ports on the pressure sensor: one is connected through the vinyl chloride tube with length of 1.5 m to a hole for pressure measurement, and the other is open to the atmospheric pressure. The difference pressure between the two ports is obtained as the output voltage when 5 V-DC is supplied. Figure 4 shows the device for multipoint pressure measurements. This measurement device consists of two cases, and each case stores 4 boards, on each of which 16 pressure sensors are arranged, so that pressure at 128 points can be measured at once.

The data from the transducers are acquired through the terminal board by a PC with two 64-channel A/D converters, so that distributions of surface-pressure data on a cylinder can be measured at the same time. Figure 5 shows the experimental setup of multipoint pressure measurements⁷⁻⁹⁾.

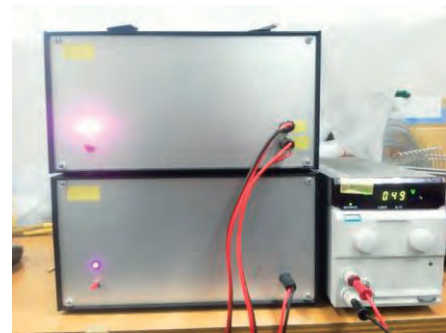


a) Sensor MS4515

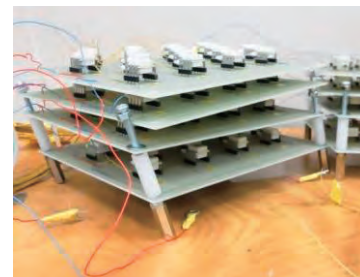


b) Output range in Voltage

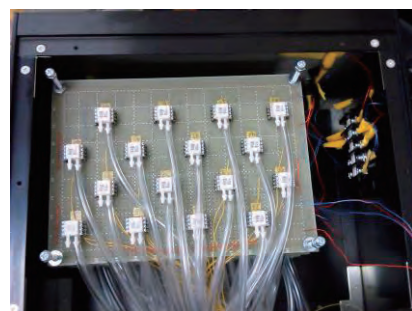
Fig.3 Output range of semiconductor pressure sensor



a) Two cases



b) four boards



c) 16 pressure sensors on board

Fig.4 Device for multipoint pressure measurements

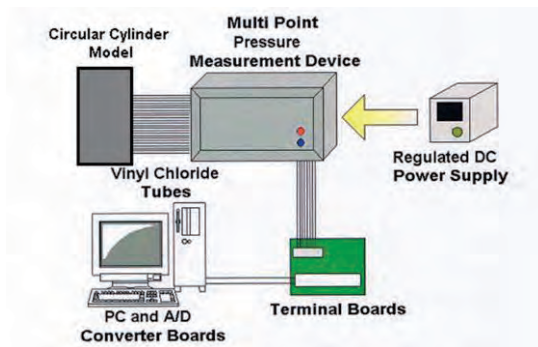


Fig.5 Setup of multipoint pressure measurements

Table 1 Speed and Re number

Wind Speed U (m/s)	Reynolds Number Re $\times 10^5$
10	1.43
15	2.14
20	2.86
25	3.57
30	4.29
35	5.00
38	5.43

2.3 Model of circular cylinder

First, the diameter of the cylinder model was decided so that critical Reynolds number about 3×10^5 should be obtained at wind speed 20 m/s, and then the polyvinyl chloride pipe with a standard size close to the above diameter was adopted. The dimension is 0.216 m in diameter (d) and 1.0 m in length (l), therefore aspect ratio l/d is 4.63. 128 holes for pressure measurements were made spirally around the cylinder surface to avoid the flow interference between adjacent holes.

Figure 6 shows setup of the circular cylinder model within the test section of the wind tunnel, where both ends of the cylinder model are attached to the parallel wall surface. In order to avoid suffering from effects of the boundary layer on the test-section wall, the pressure holes are created except 0.1 m portion for each end.



Fig.6 Model of circular cylinder

2.4 Experimental conditions

Wind speed (U) is set at interval of 5 m/s from 10 m/s to 35 m/s, and at maximum speed 38 m/s, totally in 7 patterns (see Table 1), and the resultant range of Reynolds number (Re) $1.4 \times 10^5 < Re < 5.5 \times 10^5$ includes the critical state $Re = 3 \times 10^5 \sim 4 \times 10^5$. In pressure measurements, the sampling frequency is 400 Hz with number of sampling points 17000, so that the total sampling range is 42.5 sec.

3. Results and Discussion

Figure 7 shows the distributions of time-averaged surface pressure coefficients (C_p) during last 5 seconds for each Reynolds number, and Fig. 8 does those of RMS (Root Mean Square) for time history of C_p at each location and condition in Fig.7. In both figures the horizontal axes are for angle θ from the stagnation point. Comparison with typical C_p distributions⁷⁾ is displayed in Fig.9. Figure 10 shows the time history of pressure-drag coefficients C_{Dp} and pressure-lift coefficients C_{Lp} computed from instantaneous C_p distributions for each flow condition of $U=10, 15, 20, 25, 30, 35$ m/s. Figure 11 shows typical results of FFT analyses for time histories of C_{Dp} and C_{Lp} in Fig.10. Figure 12 shows change of C_{Dp} calculated from the time-averaged C_p distributions during last 5 seconds, with regard to the Reynolds number, where error bars are from maximum and minimum values of instantaneous C_{Dp} during total 42.5 seconds. Figures 13 and 14 show, respectively, changes of RMS of C_{Dp} (perturbation of pressure-drag coefficients) and RMS of C_{Lp} (perturbation of pressure-lift coefficients), calculated from time history of instantaneous C_{Dp} and C_{Lp} (Fig.10) during last 5 seconds, with regard to the Reynolds number.

Figures 15 and 16 show the relations between estimated Strouhal number (St) and Reynolds number. Here Strouhal number $St = f d / U$ is estimated by use of peak frequency (frequency with peak amplitude) f in the FFT analysis. Strouhal numbers in Fig.15 are calculated from the FFT for the time history of pressure in voltage at local points (a) $\theta=84^\circ$, (b) $\theta=118^\circ$ and (c) $\theta=146^\circ$, while Strouhal numbers in Fig.16 are computed from the FFT for the time history of C_{Lp} .

3.1 Time-averaged C_p distributions

First, from Fig.12, since C_{Dp} abruptly decreases at about $Re=(2.86\sim 3.57) \times 10^5$, it is comprehended that the flow field is in the critical state for $Re=2.86 \times 10^5, 3.57 \times 10^5$, and therefore the flow field is in the subcritical state for $Re \leq 2.14 \times 10^5$ and in the supercritical state for $Re \geq 4.29 \times 10^5$.

In Fig.7, for the subcritical states for $Re \leq 2.14 \times 10^5$, C_p decreases from $\theta=0^\circ$ to the vicinity of $\theta=70^\circ$, then recovers up to 80° , and afterwards takes almost constant value $C_p \doteq -1.0$. Correspondingly RMS distributions (Fig.8) have the maximum values at about $\theta=75^\circ$. It is regarded that the laminar boundary layer is separated at about $\theta=80^\circ$ in the upstream side of the cylinder top.

However, for the critical states for $Re = 2.86 \times 10^5$ and 3.57×10^5 , C_p distributions become unsymmetrical between $\theta > 0^\circ$ and $\theta < 0^\circ$. From the observation in the time history of C_{Dp} and C_{Lp} (Fig.10) that C_{Lp} is not zero in average for the corresponding Reynolds number, it is presumed that alternate release of vortices are not made equally for $\theta > 0^\circ$ and $\theta < 0^\circ$, which is surely observed in the animation for time-dependent C_p distributions.

In the supercritical range where the Reynolds number is made higher to $Re \geq 4.29 \times 10^5$, C_p distributions become again

almost symmetrical for $\theta > 0^\circ$ and $\theta < 0^\circ$. C_p decreases abruptly down until about $\theta=80^\circ$, it is gradually recovered during $80^\circ \leq \theta \leq 105^\circ$, afterwards C_p increases at a burst for $105^\circ \leq \theta \leq 130^\circ$, and it is almost constant for $\theta > 130^\circ$.

In the critical and supercritical states the RMS distributions have two peaks for $\theta > 0^\circ$, low peaks at about $\theta=90^\circ$ and sharp peaks at about $\theta=105^\circ \sim 115^\circ$, in the vicinity of the inflection points of C_p curves, and relatively middle values during about 20° after the sharp peaks. Along with established explanation, this C_p pattern is due to the phenomenon that the boundary layer once separates at about $\theta=90^\circ$ (low RMS peak), the layer becomes turbulent, reattaches at about $\theta=105^\circ \sim 115^\circ$ (sharp RMS peak), flows along the cylinder surface, and the turbulent boundary layer is separated with vortex release in the downstream side of the cylinder top. The RMS distributions for $\theta > 0^\circ$ indicate that the reattachment points are located more downstream for the critical state than for the supercritical state.

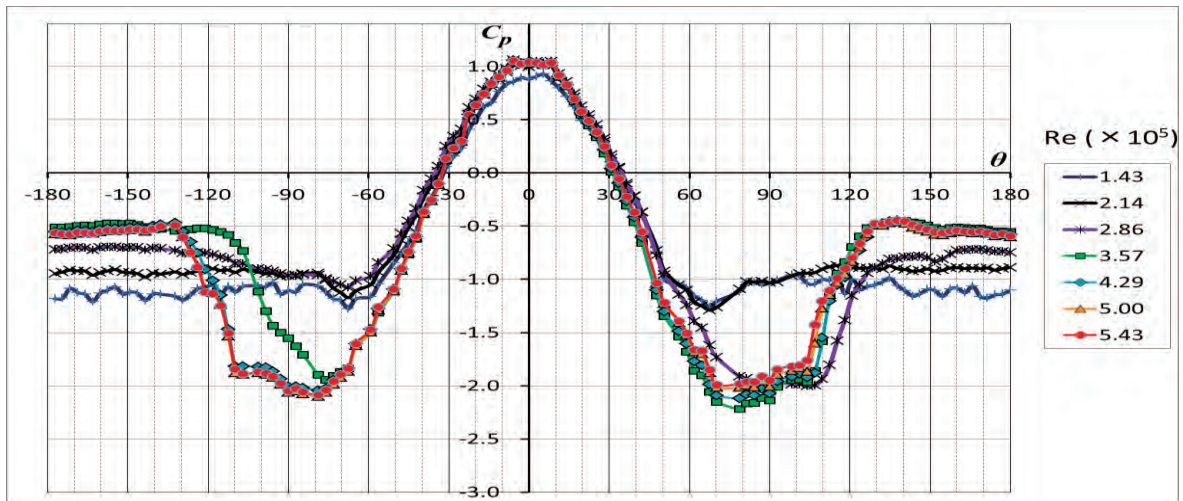


Fig.7 Distribution of mean pressure coefficients about circular cylinder

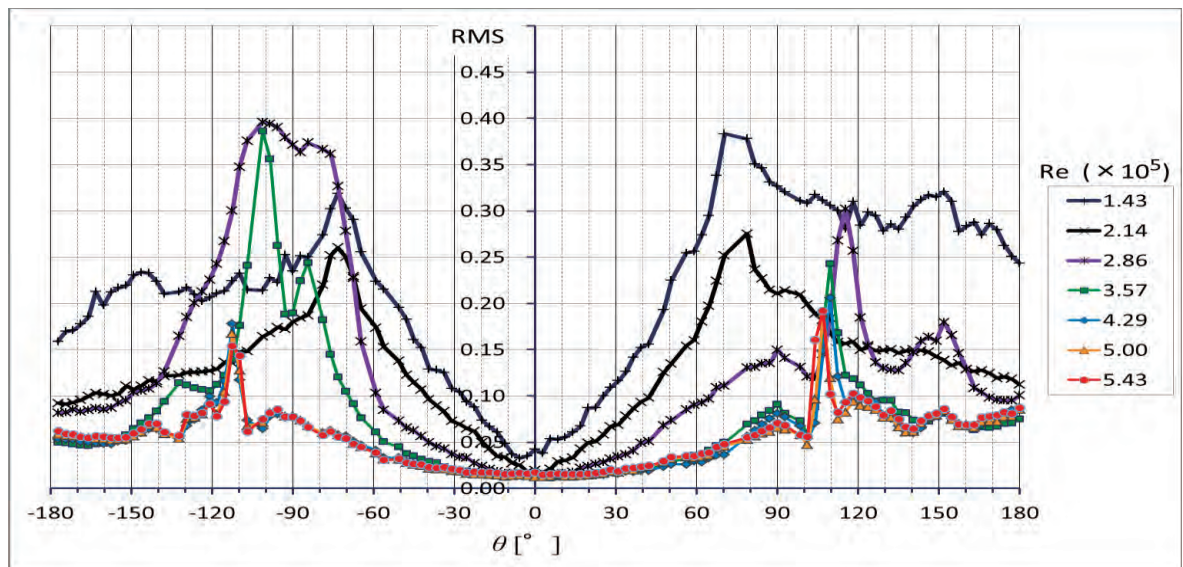


Fig.8 RMS distribution for time history of pressure coefficients about circular cylinder

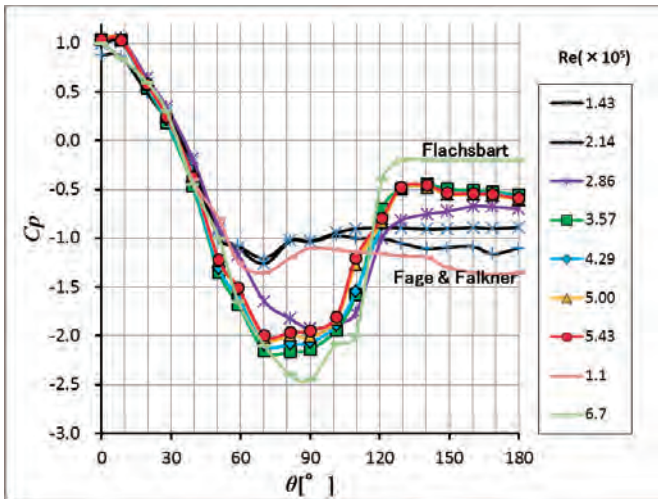


Fig.9 Comparison with typical Cp distributions

In Fig.9 comparison of Cp is shown between the present distributions (Fig.7) and typical ones⁷⁾ for $Re=1.1 \times 10^5$ (Fage & Falkner) and $Re=6.7 \times 10^5$ (Flachsbart). There is discrepancy in values, but the tendency is very similar.

3.2 Time history of C_{Dp} and C_{Lp}

About the pressure-drag coefficients in the time history shown in Fig.10, the instantaneous C_{Dp} values almost agrees, in time average, with the mean C_{Dp} values in Fig.12 computed from the time-averaged Cp distribution.

About the pressure-lift coefficients, the time history shows some characteristics. The wave shape can be regarded that oscillations with high frequency are added on a global undulation with low frequency. In the case of $Re=1.43 \times 10^5$ the amplitude of high-frequency oscillation is largest and effect of global undulation is limited. The reason would be that alternate appearance of low pressure portions by vortex shedding generates the large amplitude of lift oscillations since the laminar boundary layer is separated in the upstream side of the cylinder top. As the Reynolds number is made higher up to 2.86×10^5 , amplitude of the high-frequency component becomes smaller, and the low-frequency undulation becomes more visible, and is visibly remarkable for $Re \leq 3.57 \times 10^5$.

Actually in FFT analyses shown in Fig.11, for $Re=2.14 \times 10^5$, 2.86×10^5 there appear two peak frequencies: a low peak frequency and a normal peak frequency corresponding to the frequency of vortex shedding. The amplitude of the low frequency becomes larger as the Reynolds number increases up to $Re=2.86 \times 10^5$. For $Re=3.57 \times 10^5$ there are many lower and higher peak frequencies than the normal peak frequency. Here the normal peak frequency is specified by Strauhal number about 0.2. In Figs.11 and 16 it is observed that various

frequencies for oscillations of C_{Lp} appear for $Re \geq 3.57 \times 10^5$ where separation of the turbulent boundary layer occurs.

It is remarkable in Fig.10 that at $Re=2.86 \times 10^5$ and 3.57×10^5 in the critical state, C_{Lp} is not zero in average, which is considered that the wind leans to some direction.

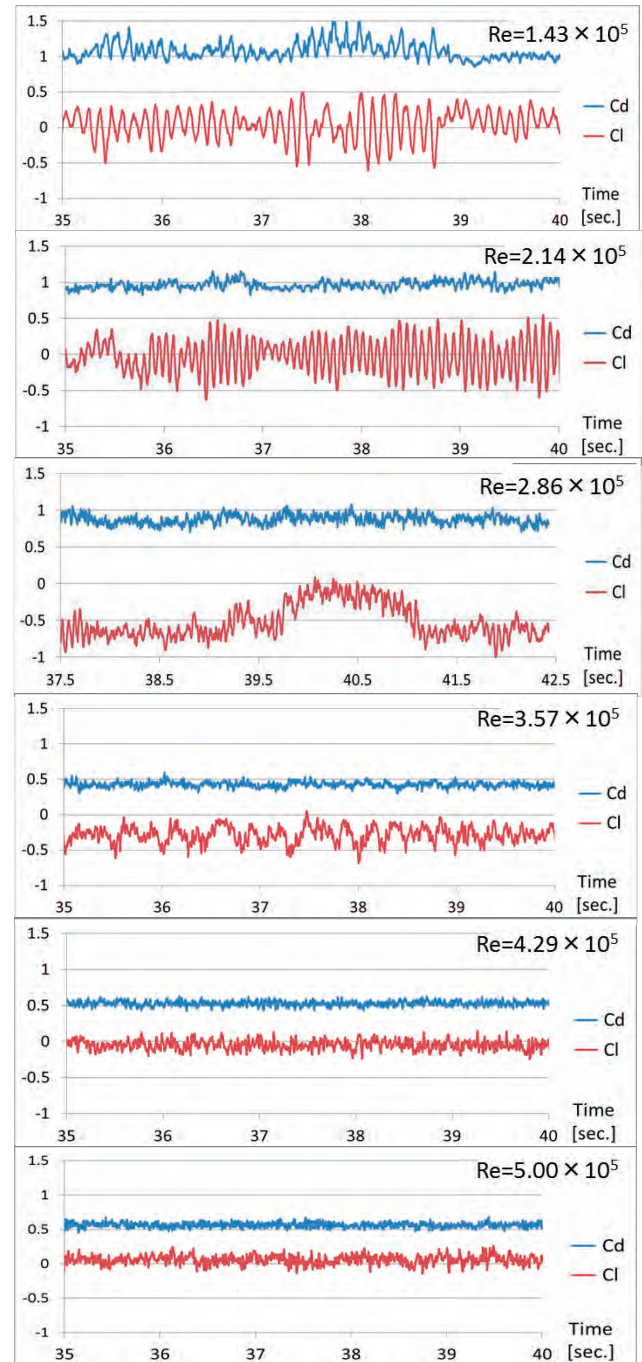


Fig.10 Time history of instantaneous C_{Dp} and C_{Lp}

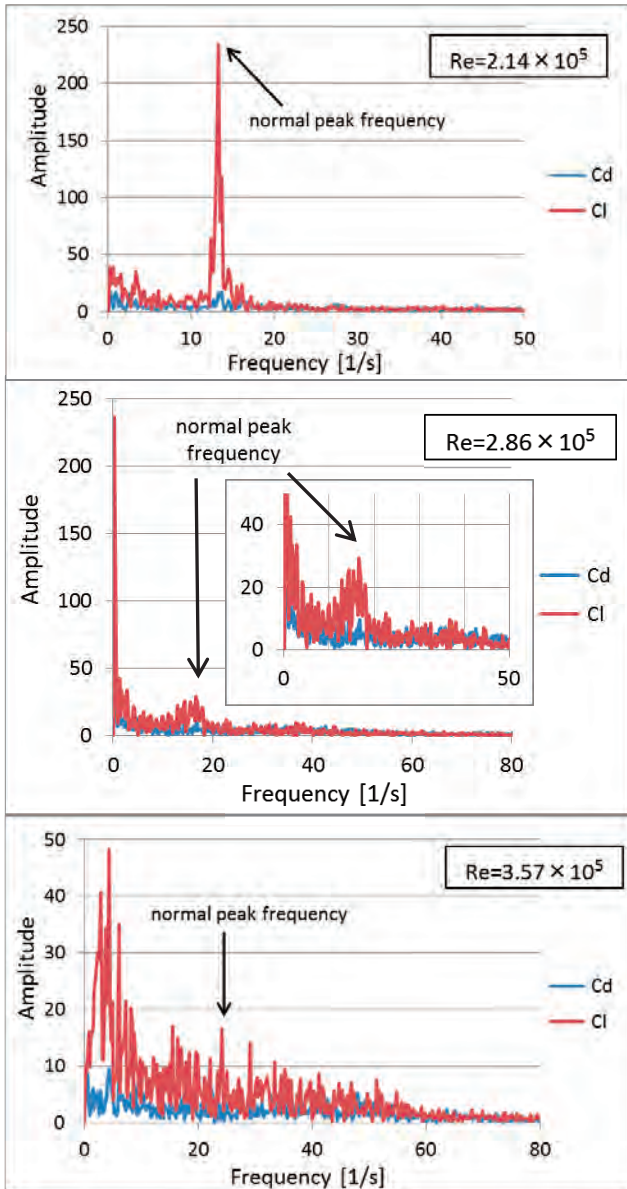


Fig.11 Results of FFT analyses for C_{Dp} and C_{Lp}

3.3 Change of C_{Dp} , RMS of C_{Lp} , and St with regard to Re

About drag coefficients of the circular cylinder, for $Re \leq 2 \times 10^5$, $C_D=0.74$ and $C_D=1.2$ in the case of aspect ratio $l/d=5$ and $l/d=\infty$, respectively, and at about $Re= 3 \times 10^5 \sim 4 \times 10^5$ the flow transitions³⁾. In the present case of $l/d=4.63$ with both cylinder ends attached to the parallel walls, where wall interference occurs, $C_{Dp}=0.8\sim 1.1$ for $Re \leq 2.86 \times 10^5$ in Fig.12. As mentioned before, since C_{Dp} abruptly decreases at about $Re=3 \times 10^5$, it is asserted that at $U=20, 25$ m/s, i.e., $Re=(2.86\sim 3.57) \times 10^5$, the flow field is in the critical state, and therefore the flow field is in the subcritical state for $Re \leq 2.14 \times 10^5$ and in the supercritical state for $Re \geq 4.29 \times 10^5$.

Regarding the perturbation of drag coefficients shown in Fig.13, RMS of C_{Dp} is very high for $Re=1.43 \times 10^5$ in the subcritical range, because the laminar boundary layer is separated in the upstream side of the cylinder top and the vortex

shedding does cause large drag oscillations. There is tendency that the drag perturbation is gradually made lower with increase of Reynolds number, except for a high value at $Re=2.86 \times 10^5$ in the critical range. Regarding the perturbation of lift coefficients shown in Fig.14, RMS of C_{Lp} is very low for $Re \geq 4.29 \times 10^5$ in the supercritical range, because the turbulent boundary layer is separated in the downstream side of the cylinder top and the vortex shedding does not cause large lift oscillations. It is notable that the change of lift perturbation indicates the same tendency as the change of the drag coefficient. Thus it is confirmed that for both drag and lift coefficients, the perturbation is locally increased in the region from the subcritical to the critical states.

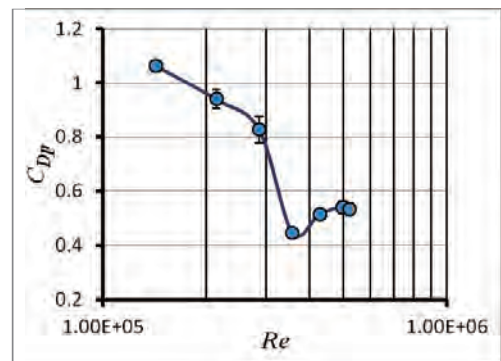


Fig.12 Change of C_{Dp} with regard to Re

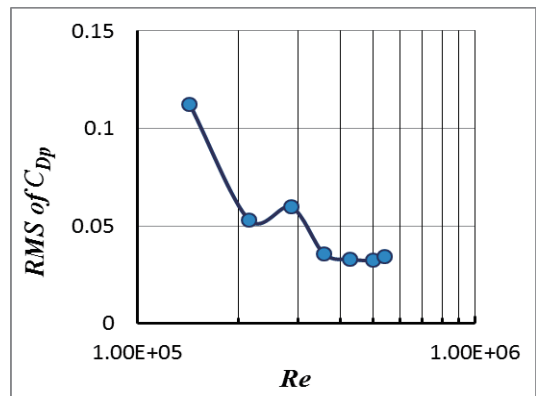


Fig.13 Perturbation of C_{Dp} with regard to Re

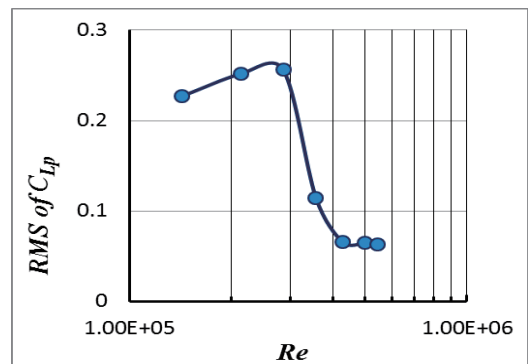
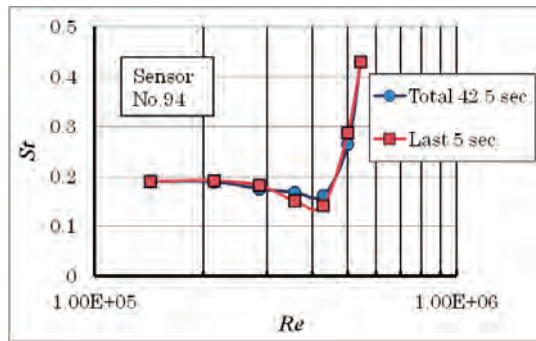
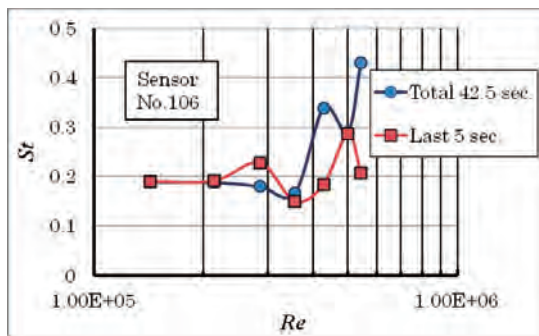


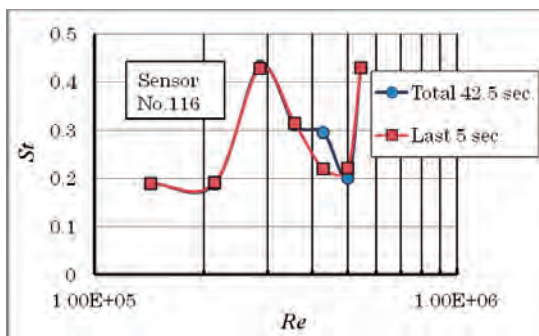
Fig.14 Perturbation of C_{Lp} with regard to Re



(a) $\theta = 84.375^\circ$ (at laminar separation point)



(b) $\theta = 118.125^\circ$ (at turbulent separation point)



(c) $\theta = 146.25^\circ$ (in separation region)

Fig.15 Change of St based on FFT for pressure in voltage

About change of Strouhal number with regard to Reynolds number, Generally it is stated²⁾ that in range of $250 < Re < 3 \times 10^5$, the Strouhal number for the vortex release is about $St = 0.19 \sim 0.21$, and it rises up to $St = 0.4 \sim 0.5$ in the Re range from the critical to the supercritical states.

Figure 15 shows the change of Strouhal number estimated by dominant frequencies (frequency with dominant peak amplitude) in the FFT for pressure history in output voltage during total 42.5 seconds and last 5 seconds at local points (a) $\theta=84.375^\circ$, (b) $\theta=118.125^\circ$, and (c) $\theta=146.25^\circ$. In three cases the Strouhal number is about 0.2 for $Re \leq 2.86 \times 10^5$ in the subcritical range, which corresponds to general statement²⁾ previously mentioned. At (a) $\theta=84.375^\circ$ in the vicinity of the separation point of the laminar boundary layer in the upstream of the cylinder top, the pressure frequency abruptly increases for $Re \geq 5 \times 10^5$ in the supercritical region. On the other hand, at (b) $\theta=118.125^\circ$ in the vicinity of the separation point of the turbulent boundary layer, the pressure frequency increases at $Re=2.86 \times 10^5$, from the subcritical to the critical region, but St depends on the duration of the FFT, which indicates that time dependency of the phenomenon is strong. At (c) $\theta=146.25^\circ$ in the separation region, the pressure frequency is always large at $Re=2.86 \times 10^5$, which implies that wake region suffers from influence of pressure perturbation at the turbulent separation point in the region from the subcritical to the critical states.

In Fig.16 change of Strouhal number for Reynolds number is shown where St is estimated by the peak frequency in the FFT results (Fig.11) for the time history of C_{Lp} (Fig.10), because the frequency of lift force directly corresponds to that of the vortex release. As is observed in Fig.11, number of peak frequencies increases for $Re \geq 3.57 \times 10^5$, from the critical to the supercritical region. Therefore in the graph Strouhal number based on the dominant frequency is marked by circle, with peak frequencies shown by triangles. It is confirmed that the change of Strouhal number shows general tendency²⁾ previously stated.

4. Conclusions

Characteristics of unsteady flows around the circular cylinder have been captured experimentally by simultaneous multipoint pressure measurement. As results the following conclusions have been obtained:

- 1) Characteristics of unsteady flows have been shown in subcritical, critical, and supercritical states. Above all, the characteristics in the critical range have been presented.
- 2) The simultaneous multipoint pressure measurements have been almost successful.

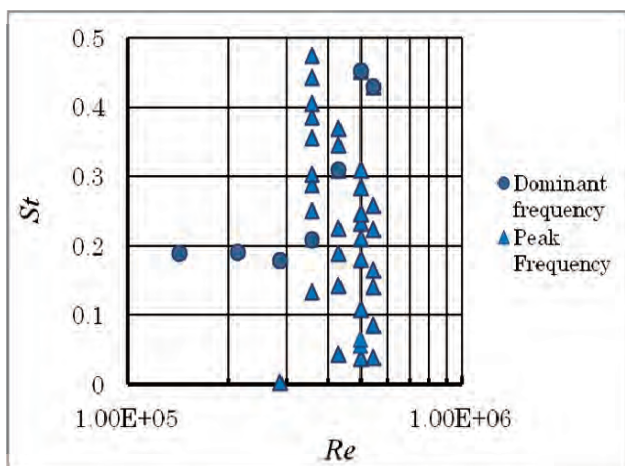


Fig.16 Change of St based on FFT for C_{Lp}

REFERENCES

- 1) Hermann Schlichting, *Boundary-Layer Theory*, McGRAW-HILL BOOK COMPANY, 1979.
- 2) *Hydrodynamic and Fluid Dynamics, Kikaikougakubinran* (in Japanese), The Japan Society of Mechanical Engineers, ed., 1976.
- 3) Yasuki, Nakayama, *Dynamics of Fluid* (in Japanese), 2011.
- 4) M. M. Zdravkovich, *Flow around Circular Cylinders*, Vols.1 and 2, Oxford University Press, 2007.
- 5) Kiyoshi Yamamoto, Numerical Wind Tunnel, *Nagare*, Japan Society of Fluid Mechanics, ed., Vol. 21, pp.429-436, 2002.
- 6) Chisachi Kato, Prospects and Problems with Computational Fluid Dynamics applied to Industrial Design in the 21st Century, *Nagare*, the Japan Society of Fluid Mechanics, ed., Vol..30, pp.57-60, 2011.
- 7) A. Roshko, Experiments on the flow past a circular cylinder at very high Reynolds numbers, *Journal of Fluid Mechanics*, Vpl.10, pp.345-356, 1961.
- 8) Yoko Takakura, Shigeru Watanabe, and Michitoshi Takagi, Unsteady Flows around a Circular Cylinder with Simultaneous Multipoint Measurements of Pressure, *Proceedings of the 11th Asian Symposium on Visualization*, ASV11-99-68, 2011.
- 9) Naotaka Watanabe, Tomohiro Furuta, and Yoko Takakura, Unsteady Flows around a Circular Cylinder with Simultaneous Multipoint Measurements of Pressure (2), *Proceedings of the 12th International Conference on Fluid Control, Measurements, and Visualization* (FLUCOME2013), OS14-03-3, 2013.
- 10) Daisuke Akiyama and Michitoshi Takagi, Unsteady Wakes of Motorcycle Scale-Models, *Proceedings of the 11th International Symposium on Flow Visualization*, Notre Dame, USA, 2004.